



OPEN ACCESS

EDITED BY

Hongfang Jin,
Peking University, China

REVIEWED BY

Ying Zhang,
China Medical University, China
Xiaojuan Ji,
Chongqing General Hospital, China

*CORRESPONDENCE

Jing Yang
✉ 1668380187@qq.com
Yu-Qi Zhang
✉ changyuyqi@hotmail.com

[†]These authors share first authorship

SPECIALTY SECTION

This article was submitted to Pediatric Cardiology, a section of the journal Frontiers in Pediatrics

RECEIVED 05 February 2023

ACCEPTED 24 March 2023

PUBLISHED 17 April 2023

CITATION

Chen L-J, Wu L-P, Zhao L-S, Zhang Z-F, Liu J-L, Hong W-J, Zhong S-W, Bao S-F, Yang J and Zhang Y-Q (2023) Comparison of cardiac function between single left ventricle and tricuspid atresia: assessment using echocardiography combined with computational fluid dynamics. *Front. Pediatr.* 11:1159342. doi: 10.3389/fped.2023.1159342

COPYRIGHT

© 2023 Chen, Wu, Zhao, Zhang, Liu, Hong, Zhong, Bao, Yang and Zhang. This is an open-access article distributed under the terms of the [Creative Commons Attribution License \(CC BY\)](https://creativecommons.org/licenses/by/4.0/). The use, distribution or reproduction in other forums is permitted, provided the original author(s) and the copyright owner(s) are credited and that the original publication in this journal is cited, in accordance with accepted academic practice. No use, distribution or reproduction is permitted which does not comply with these terms.

Comparison of cardiac function between single left ventricle and tricuspid atresia: assessment using echocardiography combined with computational fluid dynamics

Li-Jun Chen^{1†}, Lan-Ping Wu^{1†}, Lei-Sheng Zhao¹, Zhi-Fang Zhang¹, Jin-Long Liu², Wen-Jing Hong¹, Shu-Wen Zhong¹, Sheng-Fang Bao¹, Jing Yang^{3*} and Yu-Qi Zhang^{1*}

¹Department of Pediatric Cardiology, Shanghai Children's Medical Center, School of Medicine, Shanghai Jiao Tong University, Shanghai, China, ²Institute of Pediatric Translational Medicine, Shanghai Children's Medical Center, School of Medicine, Shanghai Jiao Tong University, Shanghai, China, ³Department of Ultrasound, Jiaying University Affiliated Women and Children Hospital, Jiaying, China

Patients with single left ventricle (SLV) and tricuspid atresia (TA) have impaired systolic and diastolic function. However, there are few comparative studies among patients with SLV, TA and children without heart disease. The current study includes 15 children in each group. The parameters measured by two-dimensional echocardiography, three-dimensional speckle tracking echocardiography (3DSTE), and vortexes calculated by computational fluid dynamics were compared among these three groups. Twist is best correlated with ejection fraction measured by 3DSTE. Twist, torsion, apical rotation, average radial strain, peak velocity of systolic wave in left lateral wall by tissue Doppler imaging (sL), and myocardial performance index are better in the TA group than those in the SLV group. sL by tissue Doppler imaging in the TA group are even higher than those in the Control group. In patients with SLV, blood flow spreads out in a fan-shaped manner and forms two small vortexes. In the TA group, the main vortex is similar to the one in a normal LV chamber, but smaller. The vortex rings during diastolic phase are incomplete in the SLV and TA groups. In summary, patients with SLV or TA have impaired systolic and diastolic function. Patients with SLV had poorer cardiac function than those with TA due to less compensation and more disordered streamline. Twist may be good indicator for LV function.

KEYWORDS

functional single left ventricle, tricuspid atresia, single left ventricle, cardiac function, three-dimensional speckle tracking echocardiography (3DSTE), computational fluid dynamics—CFD

Abbreviations

3DSTE, three-dimensional speckle tracking echocardiography; ASD, atrial septal defect; BSA, body surface area; CFD, computational fluid dynamics; CMR, cardiac magnetic resonance; CSaverage, average circumferential strain; DecT, deceleration time of mitral early filling wave; E, peak velocity of early filling wave of mitral inflow; EDV, end diastolic volume; E/eL, ratio of E to eL; EF, ejection fraction; eL, peak velocity of early filling wave in left lateral wall by tissue Doppler imaging; eR, peak velocity of early filling wave in right lateral wall by tissue Doppler imaging; ESV, end systolic volume; FSLV, functional single left ventricle; GCS, global circumstantial strain; GLS, global longitudinal strain; ICC, intraclass correlations; ICT, isovolumetric contraction time; IRT, isovolumic relaxation time; LSaverage, average longitudinal strain; MAPSE, mitral annular plane systolic excursion; MPI, myocardial performance index; PS, pulmonary stenosis; PH, pulmonary hypertension; Rotation_A, apical rotation; Rotation_B, basal rotation; RSaverage, average radial strain; S, strain; SI, sphericity index; sL, peak velocity of systolic wave in left lateral wall by tissue Doppler imaging; sR, peak velocity of systolic wave in right lateral wall by tissue Doppler imaging; TAPSE, tricuspid annular plane systolic excursion; TDI, tissue Doppler imaging; TGA, transposition of great artery; TSaverage, average principal tangential strain; VSD, ventricular septal defect.

Introduction

Single left ventricle (SLV) and tricuspid atresia (TA) are two common subtypes of functional single left ventricle (FSLV), a kind of complex cyanotic congenital heart disease with single or systemic left ventricle (1). Cardiac dysfunction is common in these patients during the midterm and long-term follow-up after the Fontan procedure (2).

The impact of ventricular morphology on ventricular function and clinical outcomes are controversial. Only limited studies were focused on the characteristics of different subtypes of FSLV (3–6). Altered ventricular geometry such as increased sphericity and extension of the apex resulting from overload may consequently increase ventricular function (7). Geometry, structure, and systolic function affect its filling and even diastolic function, as noted by Rösner et al. (8). Compared with SLV, TA appears to have a more ellipsoid shape of the LV. Therefore, we propose that TAs have better cardiac function than SLVs do.

Echocardiography is a reliable and convenient clinical assessment tool for ventricular function measurement (9). It has good correlations with cardiac magnetic resonance (CMR) (10) and, therefore, can be applied in FSLV (11). Computational fluid dynamics (CFD) is a new and useful method that can help visualize the fluid field inside the cardiac chamber (12). This study utilized echocardiography combined with the CFD method to assess and compare the cardiac function in children with SLV or TA, and establish good parameters for cardiac function analysis.

Methods

Subjects

Fifteen patients with SLV and 15 with TA who were diagnosed using echocardiography and confirmed by surgery from August 2015 to May 2022 in Shanghai Children's Medical Center were recruited. Children with serious arrhythmia or other conditions such as taking medicine which affects the ventricular function were excluded. The exclusion criteria were poor image quality that was inadequate for analysis. All the children had conventional two-dimensional echocardiography, three-dimensional speckle tracking echocardiography (3DSTE), and CMR examination. In addition, 3DSTE examination was performed on 15 age- and gender-matched children (Control

group), who had echocardiography examination for heart murmur but no positive finding. Characteristics of the subjects are shown in **Table 1**. Informed consent was obtained from parents of these children. The study was implemented according to the standards of the Declaration of Helsinki. The study was approved by the local institutional review board (IRB) and regional research ethics committee (REC) of the Shanghai Children's Medical Center Affiliated to Shanghai Jiao Tong University School of Medicine.

Images acquisition and analysis of echocardiography

Each of the children lay quietly, and oral chloral hydrate (50 mg/kg) was administered if necessary. Children with dextrocardia were scanned in the right decubitus position while the remaining subjects were scanned in the left lateral decubitus position, and the ECG was recorded simultaneously. The peak velocity of the early filling wave (E wave), deceleration time of the E wave (DecT) were measured by two-dimensional echocardiography. The peak velocity of systolic wave (sL) and early filling wave (eL) of left lateral wall, systolic wave (sR) and early filling wave (eR) of right lateral wall, isovolumic relaxation time (IRT), and isovolumetric contraction time (ICT) were measured by tissue Doppler imaging (TDI). MAPSE was defined as mitral annular plane systolic excursion or left lateral annular plane systolic excursion. TAPSE was defined as tricuspid annular plane systolic excursion or right lateral annular plane systolic excursion. The myocardial performance index (MPI), also called the Tei index, is widely used as a good parameter in the assessment of cardiac function in LV as well as single ventricle. This index is calculated by the ratio of total ICT and IRT to ejection time (13); it can be calculated by $(a-b)/b$, while "a" is the period starting from the end of mitral or atrioventricular valve inflow to the start of next one, and "b" is the ejection time of aortic valve. Corresponding parameters of the atrioventricular valve in the SLV group were compared with those of the mitral valve, while average values were used in single left ventricle with two atrioventricular valves. The ratio of E/e was calculated.

A Philips iE33 ultrasonic diagnostic apparatus (Philips, Andover, MA, United States), equipped with matrix-array X5-1 transducer was applied to acquire full volume image loops (14).

TABLE 1 Characteristics of subjects in this study.

	N	SLV	TA	<i>p</i> (N vs. SLV)	<i>p</i> (N vs. TA)	<i>p</i> (SLV vs. TA)
A (m)	6.600 ± 4.014	7.000 ± 3.380	6.533 ± 4.033	0.956	0.999	0.940
H (cm)	64.867 ± 9.296	64.667 ± 6.789	63.333 ± 8.981	0.998	0.873	0.902
W (kg)	6.473 ± 1.797	6.937 ± 1.642	6.260 ± 1.812	0.751	0.941	0.545
BSA (m ²)	0.345 ± 0.072	0.357 ± 0.059	0.334 ± 0.071	0.878	0.890	0.615
HR (bpm)	106.533 ± 17.844	119.400 ± 28.053	116.200 ± 21.805	0.285	0.487	0.923
SBP (mmHg)	82.067 ± 6.595	77.867 ± 3.204	76.800 ± 4.784	0.033	0.030	0.517
DBP (mmHg)	54.733 ± 5.535	49.867 ± 3.441	50.400 ± 4.290	0.013	0.025	0.850

A, age; H, height; W, weight; HR, heart rate; BSA, body surface area; SLV, single left ventricle; TA, tricuspid atresia; N: normal children.

The 3D full volume images were acquired in the apical four-chamber view with its temporal resolution over 20 frames per second and four cardiac cycles per capture, while the 2D images were acquired with its temporal resolution over 55 frames per second. The image loops were stored in a hard drive for further analysis. The clinical characteristics such as age, height, weight, and heart rate (HR) were also collected, and sphericity index (SI) were calculated as follows: $SI = D_{LV}/L_{LV}$, where D_{LV} is the diameter of the left ventricle and L_{LV} is the length of the left ventricle. TomTec 4D LV-Analysis 3 (Tomtec Imaging Systems GMBH, Unterschleißheim, Germany) was applied for post-processing analysis (15). Primary analysis were performed by manual border tracking in three planes (two-chamber, three-chamber, and four-chamber planes) (Figure 1) and then end diastolic volume (EDV), end systolic volume (ESV), stroke volume (SV), ejection fraction (EF), global longitudinal strain (GLS), global circumstantial strain (GCS), twist, torsion, apical rotation ($Rotation_A$), basal rotation ($Rotation_B$), average principal tangential strain (TSaverage), average circumferential strain (CSaverage), average longitudinal strain (LSaverage), and average radial strain (RSaverage) were automatically calculated by the software. Images that were not satisfied with automatic tracking could be manually modified and analyzed again.

Image acquisition and analysis of CMR

CMR studies were performed on a 1.5-T Intera Achieva scanner18 (Philips Medical Systems, Best, The Netherlands) on

all the patients. Retrospectively, EKG-gated balanced steady-state free precession (SSFP) cine movies were used. Slice thickness was 4–8 mm, while the interslice gap was set to zero. The temporal resolution was over 30 frames per cardiac cycle. Then images acquired were analyzed using commercial software (Philips View Forum, Andover, MA, United States).

Reconstruction and computation

Four-dimensional ECHO images were imported into medical imaging software (Materialise®-Mimics 19.0, Plymouth, MI, United States); then, we used the “Thresholding” tool to determine the appropriate gray value range to include all the left ventricle information. Then, we entered the “Edit masks” module, used the “Region growing” and “Calculate 3D from mask” tool to generate the mask and 3D model. At last, the edge was smoothed by the “Smooth mask” tool and smoothed papillary muscles and valves out. After that, the anatomy was represented by five body-fitted prism layers using the commercial software ANSYS®-ICEM 14.5; velocity obtained by two-dimensional Doppler was used as boundaries for numerical solutions of the Navier–Stokes flow equations. The distance from the first layer to the model surface was 0.02 mm, with 1,000,000 to 3,000,000 tetrahedral mesh elements filling the remaining of the calculated domain, with a tetrahedral mesh filling the remainder of the calculated domain. The blood in the LV is assumed to be an incompressible Newtonian fluid with a constant viscosity of

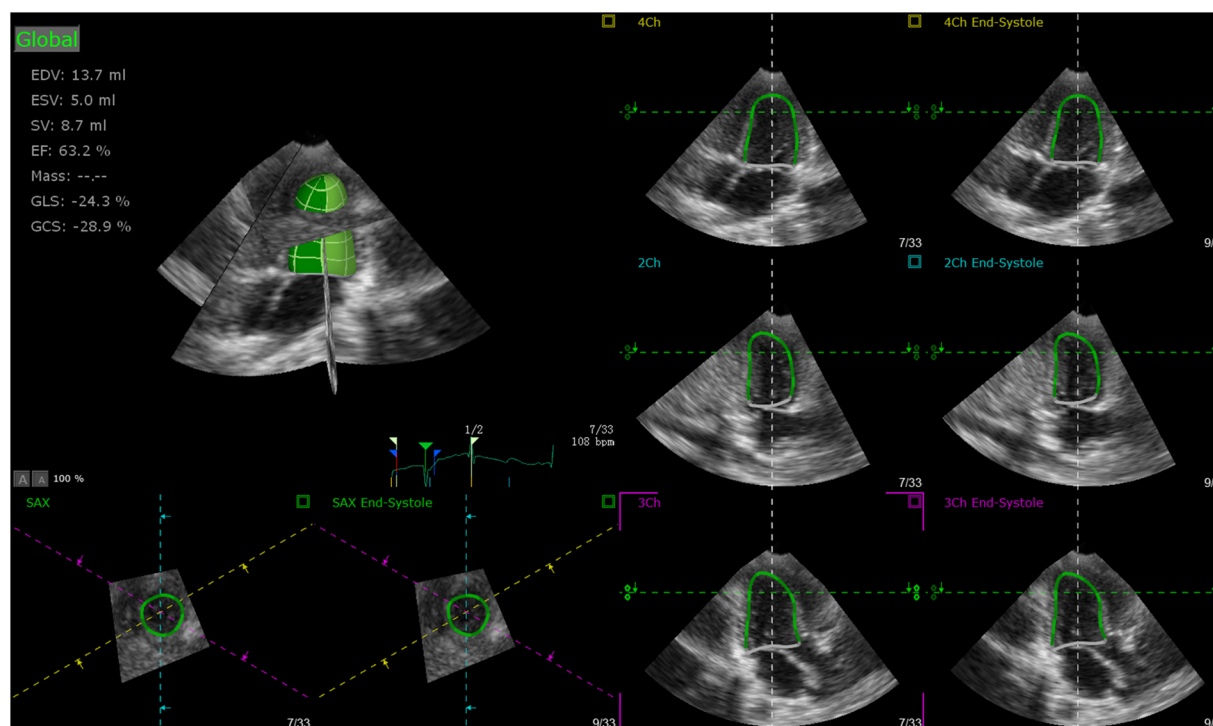


FIGURE 1 Primary analysis performed by manual border tracking in three planes (two-chamber, three-chamber, and four-chamber).

0.004 kg/ms and density of 1,060 kg/m³. The second-order upwind scheme was employed to complete the steady-state numerical simulation by ANSYS®-ICEM 17.0 software. The standard *k* - ϵ model was employed to solve the motion of intraventricular blood flow inside the ventricle. The results were analyzed and processed by ANSYS CFD-Post 14.5 software.

Statistical analysis

Statistical Package for Social Sciences (SPSS 17.0, SPSS Inc., Chicago, IL, United States) was applied for statistical analysis. Quantitative variables were presented as mean \pm SD and compared with *t*-test and Mann–Whitney test between groups. A two-sided *p*-value <0.05 was considered statistically significant. The intraclass correlations (ICCs) (16) of intraobserver and interobserver variability were used to test the reproducibility of 3DSTE. Bland–Altman analysis was used to access the bias and 95% limits of agreement for EDV, ESV, SV, and EF between 3DSTE and CMR. Pearson’s correlation coefficient was used to

access the correlation between 3DSTE parameters and EF derived from 3DSTE.

Results

Fifteen patients with SLV (SLV group) and 15 patients with TA (TA group) underwent echocardiography examination. There were no missing data during the study. In addition, 3DSTE examination was performed on 15 age- and gender-matched children (Control group). Then, statistical analysis was performed between patients and controls. Concomitant malformation in SLV group and TA group data is shown in **Table 2**. Fifteen patients with SLV (100%) and 15 with TA (100%) have ventricular septum defect (VSD). Seven with SLV (46.7%) and 14 with TA (93.3%) have atrial septal defect (ASD), while the one who did not have ASD had single atrium. Five with SLV (33.3%) and five with TA (33.3%) have pulmonary stenosis (PS). Five with SLV (33.3%) and three with TA (20%) have pulmonary hypertension (PH). Twelve of the SLVs have transposition of great artery (TGA) (80%). More detail can be seen in **Table 2**.

TABLE 2 Concomitant malformation in the SLV and TA groups.

	VSD	ASD/PFO	PS	PH	TGA	PDA	PA	Dextrocardia	Others
SLV1	+	+			+				
SLV2	+		+		+				
SLV3	+			+	+				Moderate atrioventricular regurgitation, Bilateral superior vena cava
SLV4	+		+			+			Atrioventricular valve stenosis
SLV5	+			+	+	+			IAA
SLV6	+			+	+				Atrioventricular valve stenosis
SLV7	+	+	+		+			+	
SLV8	+	+	+		+				
SLV9	+	+				+	+	+	Cor triatriatum sinister
SLV10	+	+			+	+			
SLV11	+				+				Bilateral superior vena cava
SLV12	+			+	+	+			AVSD, moderate atrioventricular regurgitation
SLV13	+	+	+		+	+			
SLV14	+	+		+	+	+			
SLV15	+					+	+		
TA1	+	+				+			
TA2	+	+	+			+			
TA3	+	+		+					
TA4	+	+				+			
TA5	+	+	+						Right aortic arch
TA6	+	+		+					SA, TAPVD
TA7	+	+				+			RVOTO, persistent left superior vena cava
TA8	+	+	+						
TA9	+	+							Persistent left superior vena cava
TA10	+	+					+		
TA11	+	+		+					
TA12	+	+	+						
TA13	+						+		SA, aorta originates from the right ventricle
TA14	+	+				+	+		
TA15	+	+	+			+			Right aortic arch

ASD, atrial septal defect; AVSD, atrioventricular septal defect; IAA, interruption of aortic arch; PA, pulmonary atresia; PDA, patent ductus arteriosus; PFO, patent foramen ovale; PS, pulmonary stenosis; PH, pulmonary hypertension; RVOTO, right ventricular outflow tract obstruction; SA, single atrium; SLV, single left ventricle; TA, tricuspid atresia; TAPVD, total anomalous pulmonary venous drainage; TGA, transposition of great artery; VSD, ventricular septal defect.

There are no significant differences in age, height, weight, body surface area (BSA), and HR among the three groups (Table 1). Diastolic blood pressure (DBP) and systolic blood pressure (SBP) are lower in both SLV and TA groups than those in the Control group ($p < 0.05$), but they are all within the normal range. The Bland–Altman plot revealed almost no bias between EDV, ESV, SV, and EF measured by 3DSTE and CMR (Figure 2).

2D echocardiography

As is shown in Table 3, there are no significant differences in E, sL, eL, E/eL, eR, ICT, and MAPSE between the SLV and the Control groups. While sR and TAPSE are poorer in the SLV group ($p < 0.05$ for sR, $p < 0.01$ for TAPSE), IRT, DecT, and MPI are larger in the SLV than in the Control group ($p < 0.01$). There are no significant differences in E, eL, E/eL, sR, ICT, DecT, and MAPSE between the TA group and the Control group. eR and TAPSE are smaller in the TA group than those in the Control group ($p < 0.05$ for eR, $p < 0.01$ for TAPSE). sL, IRT, and MPI are larger in the TA group than in the Control group ($p < 0.01$ for sL, $p < 0.05$ for IRT and MPI). There are no significant differences in E, eL, E/eL, sR, eR,

IRT, ICT, DecT, TAPSE, and MAPSE between the SLV and the TA groups, while MPI is larger in the SLV group ($p < 0.05$) and sL is larger in the TA Group ($p < 0.05$).

3DSTE

The ICCs of 3DSTE in 45 children are shown in Table 4. The intraobserver and interobserver variability are good. Intraobserver and interobserver variations are within the clinically acceptable ranges, confirming the repeatability of 3DSTE. Our results show a good consistency between 3DSTE and CMR (Figure 2), and the intraclass correlation of EDV, ESV, SV, and EF between 3DSTE and CMR are 0.995, 0.989, 0.992, and 0.879, respectively. The correlation between EF derived from 3DSTE and other parameters are shown in Figure 3. The r value of GLS, GCS, twist, torsion, Rotation_A, Rotation_B, TSaverage, CSaverage, LSaverage, and RSaverage are -0.579 , -0.540 , 0.746 , 0.594 , 0.432 , -0.675 , -0.363 , -0.538 , -0.316 , and 0.479 , respectively. Twist is best correlated with EF measured by 3DSTE.

As shown in Table 3, SI, EDV, ESV, and SV are larger, and EF, GLS, GCS, twist, torsion, Rotation_A, Rotation_B, TSaverage,

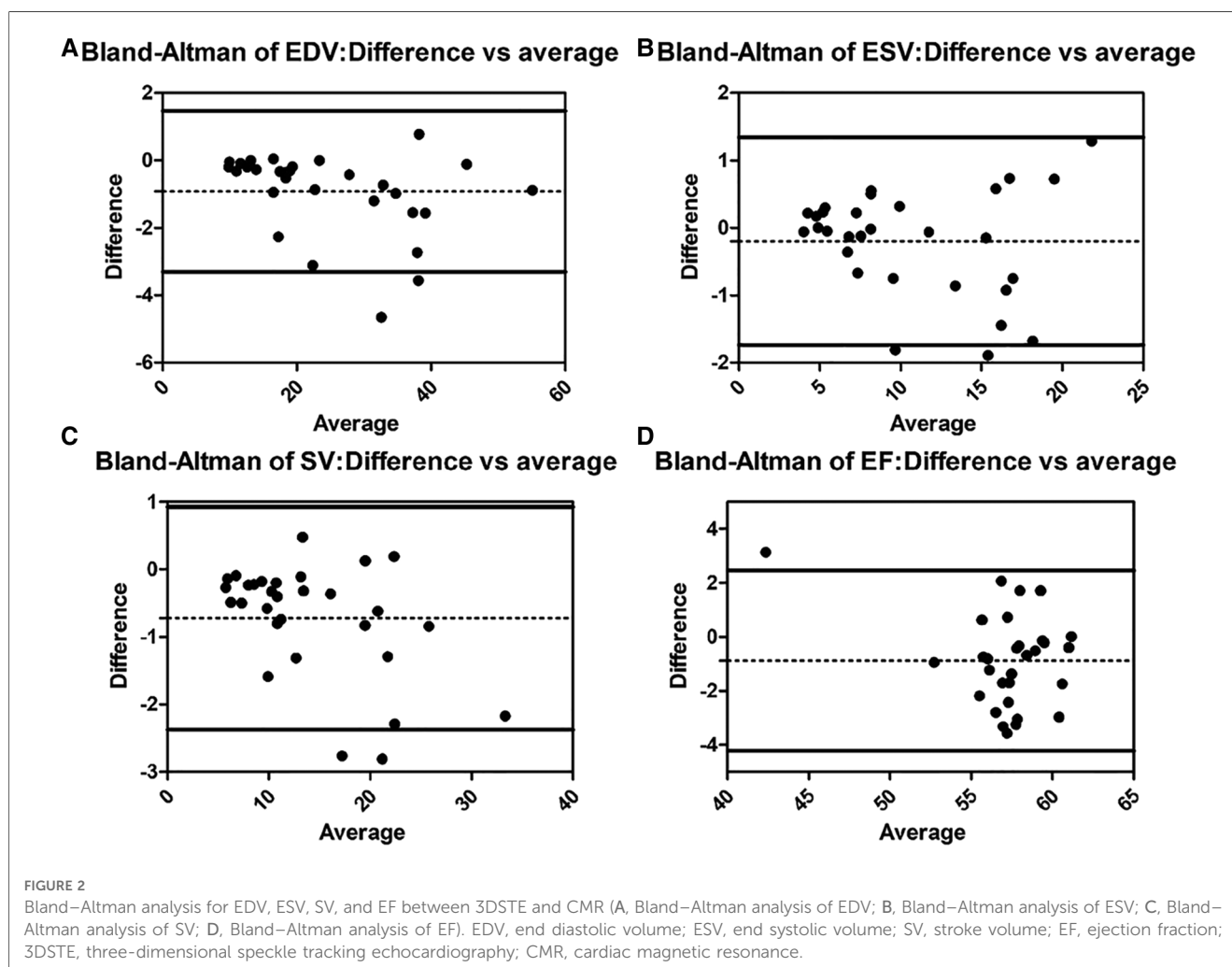


TABLE 3 Parameters of left ventricular function in patients and controls.

	N	SLV	TA	<i>p</i> (N vs. SLV)	<i>p</i> (N vs. TA)	<i>p</i> (SLV vs. TA)
SI	0.667 ± 0.031	0.960 ± 0.169	0.871 ± 0.122	0.000	0.000	0.074
EDV (ml)	12.951 ± 2.384	27.609 ± 12.456	21.089 ± 10.350	0.000	0.000	0.130
ESV (ml)	4.506 ± 1.027	12.280 ± 5.525	8.911 ± 4.479	0.000	0.000	0.065
SV (ml)	8.444 ± 1.487	15.329 ± 7.144	12.178 ± 5.913	0.000	0.005	0.206
EF (%)	65.389 ± 3.119	55.626 ± 3.696	57.887 ± 2.112	0.000	0.000	0.117
GLS (%)	-28.349 ± 2.625	-22.950 ± 3.527	-25.081 ± 3.311	0.000	0.020	0.170
GCS (%)	-29.537 ± 3.934	-23.030 ± 4.154	-25.304 ± 3.876	0.000	0.016	0.274
Twist (°)	12.615 ± 1.569	5.269 ± 2.342	7.603 ± 1.930	0.000	0.000	0.006
Torsion (°/cm)	3.273 ± 0.374	1.437 ± 0.712	2.016 ± 0.557	0.000	0.000	0.020
Rotation _A (°)	5.470 ± 1.583	1.740 ± 2.139	3.547 ± 1.864	0.000	0.020	0.031
Rotation _B (°)	-7.145 ± 1.052	-3.529 ± 1.821	-4.055 ± 1.564	0.000	0.000	0.061
TSaverage (%)	-38.270 ± 2.237	-30.701 ± 4.326	-31.913 ± 5.276	0.000	0.000	0.431
CSaverage (%)	-29.441 ± 4.133	-22.857 ± 2.847	-25.240 ± 2.923	0.000	0.004	0.139
LSaverage (%)	-27.153 ± 2.051	-23.113 ± 2.843	-24.818 ± 2.449	0.000	0.034	0.154
RSaverage (%)	46.758 ± 2.891	39.362 ± 3.887	40.545 ± 3.647	0.000	0.000	0.627
E	97.713±9.332	89.907±29.144	93.520±24.022	0.332	0.534	0.714
sL	6.115 ± 0.798	6.293 ± 1.729	7.463 ± 2.113	0.678	0.165	0.038
eL	10.161 ± 2.081	10.200 ± 5.251	11.548 ± 4.794	0.604	0.612	0.384
E/eL	9.670 ± 2.045	12.055 ± 6.373	9.553 ± 3.860	0.633	0.627	0.395
sR	10.658 ± 1.962	8.141 ± 4.016	9.225 ± 1.995	0.049	0.356	0.550
eR	14.080 ± 2.154	11.605 ± 5.846	10.233 ± 4.825	0.011	0.008	0.575
IRT	68.200 ± 12.318	81.667 ± 12.726	79.067 ± 9.035	0.007	0.234	0.810
ICT	68.600 ± 14.613	66.533 ± 18.063	66.800 ± 13.154	0.929	0.945	0.999
AduT	95.867 ± 18.267	121.111 ± 20.811	115.444 ± 19.882	0.012	0.059	0.811
DecT	77.867 ± 17.824	101.333 ± 20.486	93.867 ± 27.790	0.017	0.137	0.636
TAPSE	16.433 ± 4.370	10.981 ± 2.766	10.743 ± 2.660	0.000	0.000	0.979
MAPSE	10.239 ± 1.556	9.386 ± 2.394	9.846 ± 2.434	0.287	0.622	0.564
MPI	0.309 ± 0.048	0.477 ± 0.108	0.390 ± 0.105	0.000	0.051	0.034

SI, sphericity index; EDV, end diastolic volume; ESV, end systolic volume; EF, ejection fraction; GLS, global longitudinal strain; GCS, global circumstantial strain; Rotation_A, apical rotation; MPI, myocardial performance index; Rotation_B, basal rotation; TSaverage, average principal tangential strain; CSaverage, average circumferential strain; LSaverage, average longitudinal strain; RSaverage, average radial strain; SV, stroke volume; IRT, isovolumic relaxation time; DecT, deceleration time of mitral early filling wave; TAPSE, tricuspid annular plane systolic excursion; MAPSE, mitral annular plane systolic excursion; E: peak velocity of early filling wave of mitral inflow; sL: peak velocity of systolic wave in left lateral wall by tissue doppler imaging, eL: peak velocity of early filling wave in left lateral wall by tissue doppler imaging; sR: peak velocity of systolic wave in right lateral wall by tissue doppler imaging; eR: peak velocity of early filling wave in right lateral wall by tissue doppler imaging; ICT: isovolumic contraction time, AduT: duration time of A wave.

TABLE 4 Intraobserver and interobserver variations of 3DSTE.

	Intraobserver variability		Interobserver variability	
	ICC	<i>p</i>	ICC	<i>p</i>
EDV	0.988 (0.977–0.993)	0.000	0.962 (0.932–0.979)	0.000
ESV	0.982 (0.968–0.990)	0.000	0.960 (0.928–0.978)	0.000
SV	0.977 (0.959–0.987)	0.000	0.956 (0.921–0.976)	0.000
EF	0.771 (0.618–0.867)	0.000	0.824 (0.702–0.900)	0.000
GLS	0.828 (0.708–0.902)	0.000	0.767 (0.613–0.865)	0.017
GCS	0.808 (0.677–0.890)	0.000	0.808 (0.643–0.901)	0.000
Twist	0.884 (0.799–0.935)	0.000	0.871 (0.778–0.927)	0.000
Torsion	0.800 (0.663–0.885)	0.000	0.827 (0.706–0.901)	0.000
Rotation _A	0.984 (0.967–0.992)	0.000	0.862 (0.762–0.921)	0.000
Rotation _B	0.798 (0.661–0.884)	0.000	0.716 (0.537–0.833)	0.000
TSaverage	0.783 (0.638–0.875)	0.000	0.784 (0.639–0.875)	0.000
CSaverage	0.835 (0.719–0.906)	0.000	0.799 (0.662–0.884)	0.000
LSaverage	0.757 (0.597–0.859)	0.000	0.814 (0.686–0.893)	0.000
RSaverage	0.850 (0.743–0.915)	0.000	0.785 (0.641–0.876)	0.000

3DSTE, three-dimensional speckle tracking echocardiography; EDV, end diastolic volume; ESV, end systolic volume; EF, ejection fraction; GLS, global longitudinal strain; GCS, global circumstantial strain; Rotation_A, apical rotation; Rotation_B, basal rotation; TSaverage, average principal tangential strain; CSaverage, average circumferential strain; LSaverage, average longitudinal strain; RSaverage, average radial strain; ICC, intraclass correlation coefficient.

CSaverage, LSaverage, and RSaverage are poorer in the SLV group (*p* < 0.01) than those in the Control group. SI, EDV, ESV, and SV are larger, and EF, GLS, GCS, Twist, Torsion, Rotation_A, Rotation_B, TSaverage, CSaverage, LSaverage, and RSaverage are poorer in the TA group than those in the Control group (*p* < 0.05 for GLS, GCS, Rotation_A, and LSaverage, *p* < 0.01 for others). The differences in SI, EDV, ESV, SV, EF, GLS, GCS, TSaverage, LSaverage, and RSaverage are not significant between the SLV group and the TA group. However, twist, torsion, and Rotation_A are poorer in SLV Group (*p* < 0.01 for Twist, *p* < 0.05 for Torsion and Rotation_A).

CFD

As shown in **Figures 4, 5**, vortices differ a lot among the three groups. In normal left ventricle, during diastolic period, blood flows through the mitral valve and goes forward until reaching the apex, and then it swirls and goes backward, forming a major vortex in the middle of the left ventricle, with a counterclockwise rotation. After that, a vortex ring is formed in the base region of LV, and then, blood goes to the outflow tract region and forms a

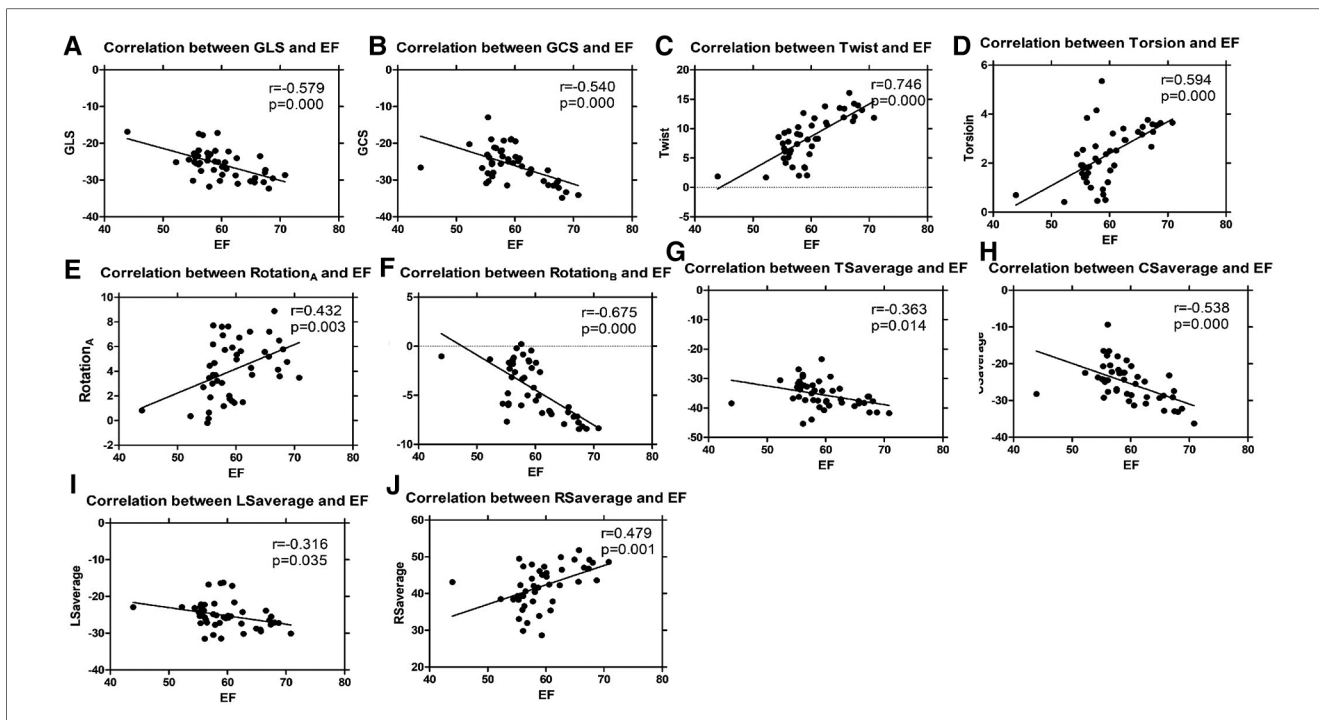


FIGURE 3 Linear regression analyses of 3DSTE parameters and EF by 3DSTE (A, GLS vs. EF; B, GCS vs. EF; C, Twist vs. EF; D, Torsion vs. EF; E, Rotation_A vs. EF; F, Rotation_B vs. EF; G, TSaverage vs. EF; H, CSaverage vs. EF; I, LSaverage vs. EF; J, RSaverage vs. EF). 3DSTE, three-dimensional speckle tracking echocardiography; EF, ejection fraction; GLS, global longitudinal strain; GCS, global circumstantial strain; Rotation_A, apical rotation; Rotation_B, basal rotation; TSaverage, average principal tangential strain; CSaverage, average circumferential strain; LSaverage, average longitudinal strain; RSaverage, average radial strain.

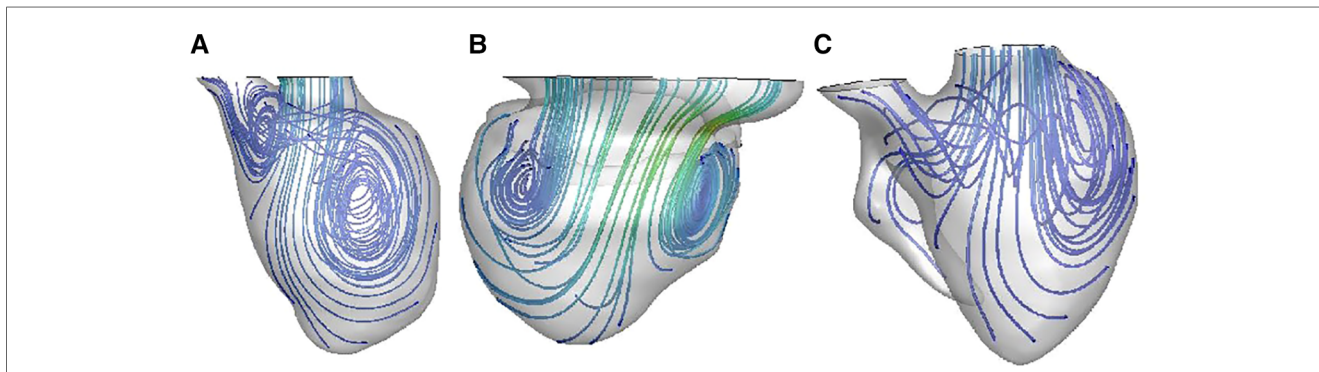


FIGURE 4 Blood streamlines in ventricular chamber in normal heart (A), patient with SLV (B), and patient with TA (C).

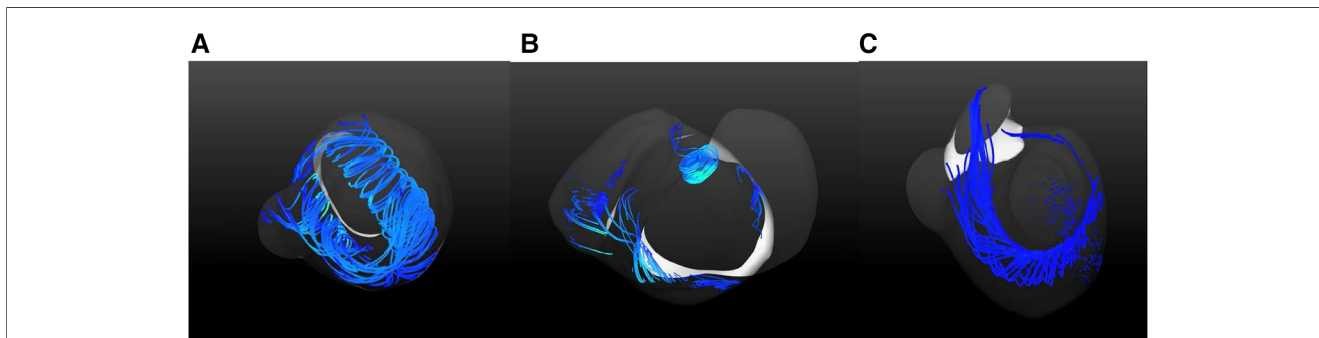


FIGURE 5 Vortex rings in LV in normal heart (A), SLV (B) and TA (C).

small clockwise rotation vortex. This is a consecutive and interactive process. In patients with SLV, blood flows straight ahead to the apex, and it spreads out in a fan-shaped manner and form two small vortices. When viewed from the front, it is clockwise on the left and counterclockwise on the right in the base region of the LV. The vortex ring during the diastolic phase is incomplete. In the TA group, the main vortex is similar to the one in the normal LV chamber, but smaller, and its center is closer to the apex and the lateral side. The vortex ring during diastolic phase is incomplete.

Discussion

In patients with SLV and TA, abnormal systolic and diastolic function are common, but they are usually evaluated separately. A previous study had implied that impaired relaxation may result from decreased systolic motion (17). In reality, systolic function and diastolic function are closely interrelated, while contractility is impaired; elastic recoil in early diastole may be also impaired too. Systolic function contributes to diastolic function through restoring forces or diastolic recoil of the myocardium from tension produced in systole. Energy stores during systolic twisting and releases during diastolic untwisting; therefore, ventricular relaxation and early diastolic filling are finished. On the other hand, since ejection depends a lot on enough filling during diastole through the Frank–Starling mechanism, diastolic function also affects contraction. Actually, both systolic and diastolic function are impaired before surgery in patients with FSLV.

Similarities between the SLV group and the TA group

2D echocardiography

There are no significant difference in E/eL ratios among these three groups, similar to the study by Hershenson et al. (18), indicating that end diastolic pressures are not increased in SLVs or TAs; some other studies also show weak correlation between E/e and filling pressures (19). Although the E/eL ratio is a common parameter to evaluate diastolic function in adults, it may be less valuable in children as it reflects elevated filling pressures, which may be less common in children (20). In our study, relatively younger age and relatively normal left lateral wall motion, resulting to relatively normal MAPSE.

Patients in both SLV and TA groups have prolonged IRT than those in the Control group. Prolongation of isovolumic time is likely to be affected by the slow rate of ventricular relaxation resulting from decline in the change rate of ventricular pressure or decrease in ventricular compliance. Such changes are likely correlated to abnormal myocardial untwisting. As presented by Appleton et al. (21), longer IRT is associated with impaired relaxation and normal filling pressures, and is the earliest and commonest change seen with diastolic abnormality.

Patients with FSLV have higher MPI and lower TAPSE values than those in the Control group, similar to previous studies (22,

23). MPI depends on events during isovolumetric contraction, ejection, and isovolumetric relaxation, and its increase reflects impaired systolic and/or diastolic function. The decrease of TAPSE reflects impaired myocardial motion of the right lateral wall.

3DSTE

Patients in the SLV and TA groups had enlarged EDV, ESV, and SV, which are consistent with previously reports (10). SLV and TA have shared characteristics: the domination of left ventricle and hypoplastic right ventricle. A previous study on angiography reported that LV dysfunction was a consequence of longstanding LV volume overload (24). LVs in both TA and SLV are overloaded because of the hypogenesis of RV; therefore, the left ventricles have to bear much more work than they usually do. The ventricular volume increases as a response aiming to maintain the normal cardiac output. Initially, though patients with SLV and TA have abnormal relaxation and impaired systolic function, EF is preserved. Subsequently, these adaptive mechanisms become insufficient, and the ventricle gradually evolves into decompensation, and at last, evident global pump dysfunction.

An experimental study (25) showed the volume overload could increase the collagen deposition in the pressure-overloaded ventricle, causing myocardial stiffness. On histologic examination, the gross pathologic change of increased LV volume is considered to be driven by the cardiomyocyte hypertrophy and apoptosis as well as the increased interstitial collagen (26).

Not surprisingly, strain values in FSLV children are significantly poorer than those in the Control group, which are consistent with previous reports (27). In normal ventricle, the myofibers are oriented in three broad layers: the superficial fibers are oriented obliquely, the middle fiber circumferentially, and the deep layer runs longitudinally (28). Myocardium contracts and relaxes with the fiber shortening and extension parallel to its orientation. While in the case of FSLV, fibers are “irregular” (29), the irregular orientation of subepicardial fibers may lead to lower circumferential strain and radial strain (30). The lower value of strain in FSLV patients can indicate nonischemic fibrosis, which is validated by late gadolinium enhancement and histologic findings (31, 32).

Myocardial fibrosis in FSLV is also an underlying reason for its impaired cardiac function, which is confirmed by cardiac magnetic resonance imaging (33). Myocardial fibrosis is intrinsically linked to LV stiffness and chamber modification (34) and is a common final pathway in chronic myocardial disease and is the structural correlate of heart failure (35). At the histological level, the myocardium of SLV has been shown to be more fibrotic than normal (36). This may explain, at least partially, the clinical observation of the abnormal performance at an early age of FSLV.

Our study also showed poorer twist, torsion, apical, and basal rotation in children with FSLV when compared with controls, as previous reported (11, 37), and may be reflective of their different fiber orientations. Rotation, torsion, and twist play an important role in both systolic and diastolic function; they distribute stress and energy across the ventricle and enhance

ventricular filling by restoring potential energy and diastolic elastic recoil during ejection. Twist is the net difference in rotation of the LV apex and base and plays an important role in LV mechanics (38). Untwist, the subsequent recoil of twist, can release the restored forces, impacting LV diastolic relaxation and early diastolic filling; these may be early signs of cardiac dysfunction before clinical symptom.

CFD

In a normal left ventricle, myocardial relaxation and contraction push blood flow with gyratory motion. The geometry and myofiber orientation of a normal left ventricle are optimized to eject blood in the systole with least energy dissipation and stored potential energy for untwisting; by untwisting, blood is effectively sucked into the ventricle. Recoiling during diastole allows the myocardium to relax and suck blood from left atrium into left ventricle, with vortices and vortex rings formed in LV, which can redirect the flow and preserve energy. It can provide dynamic energy sources for blood to flow forward, forming vortices, which can convert vortex kinetic energy into the rotational kinetic energy, and avert convective deceleration. Natural asymmetric geometry of the heart could minimize dissipative interaction of flow convection to arrange the flow for ejection.

While in patients with FSLV vortices in ventricular chambers are smaller and rounder, and even disappear, the vortex ring during the diastolic phase is incomplete. The enlarged dominant chamber, hypoplastic residual cavity and the symmetric geometry make the structure of FSLV significantly different from normal LV; therefore, the streamline inside the ventricle is disordered and flows without enough swirling, resulting in smaller vortex and incomplete vortex ring. Thus, more energy dissipates, and more performance is needed to maintain proper stroke volume.

Therefore, the abnormal orientation of the myofiber, fibrosis of myocardium, special geometry, and disordered flow fields, along with the overload of the LV, may cause weakness of contractility in systole as well as diastole, deteriorating the ventricular performance.

Differences between the SLV group and the TA group

2D echocardiography

It is notable that sL is larger in the TA group compared with the SLV group, and even the Control Group, indicating that the left lateral wall in the TA group contributes more to cardiac function, which may reflect adaptation and compensation; it may also explain the better performance in the TA group than in the SLV group. Patients in the TA group also had higher sR value than those in the SLV group, indicating that cardiac motion in the right lateral wall in the TA group are better than the SLV group, similar to a previous study (30).

Compared with the Control group, patients in the SLV group have more prolonged DecT; the difference is significant, while the difference between the TA group and the Control group is

not significant, reflecting decreased ventricular compliance in early diastolic period in SLV than in TA. As stated by Thomas and Weyman (39), impairment of LV relaxation results in the prolongation of IRT, DecT, and lower E.

Though without significant difference, there is a trend toward lower values of E in the SLV group than the TA and Control groups. Lower E is suggestive of volume overload and increased atrial reliance during diastolic in TA for ventricular filling, similar to the study by Khoo et al. (40). This increased contribution on atrial active function is a compensatory of ventricular diastolic dysfunction. Different from a normal atrium, atrial contractility plays an important role in these patients and acts as a contributor to more passive conduit properties. One possibility for this may be an indicator of the abnormal diastolic properties as previously mentioned (41) and the compensatory function of the atrium. This has been clearly demonstrated in adult studies where atrial properties are affected by ventricular diastolic abnormalities (42).

3DSTE

Compared with the TA group, patients in the SLV group have poorer twist, torsion, and rotation. The orientation of myofibers is more longitudinal in TA, with interstitial fibrous deposition greater than normal heart in all sites analyzed (43); this was found in the first weeks of life and increases with age, as found in a previous study (44), while the superficial fibers are circumferentially oriented in SLV (45). Though similar in volume overload and more spherical shape than normal children, LVs in TA and SLV have different characteristics; though not significant, SI in the SLV group is larger than the TA group. As shown in **Table 3** and **Figure 3**, twist is well correlated with EF and can help distinguish TA group from SLV group sensitively; therefore, twist may be a good measure for the assessment of ventricular performance.

CFD

The shape of the ventricle may affect a lot in the turning of streamlines and the formation of the vortices. Compared with the TA group, LV in the SLV group has rounder apex and more symmetrical structure, while it is more ellipsoidal and asymmetrical in TA. In patients with SLV, blood flows straight ahead to the apex without enough swirling; when the blood flow reaches the enlarged part in the middle of the main cardiac cavity, it spreads out in a fan-shaped manner and forms two small vortices. When viewed from the front, it is clockwise on the left and counterclockwise on the right in the base region of LV. More energy dissipates during this period. The unnatural asymmetry flow could reduce the efficiency of the heart pump by more than 10% (46). In the TA group, the main vortex is similar to the one in a normal LV chamber, but smaller, and its center is closer to the apex and the lateral side. We cautiously speculate that the obtuse apex as well as the more symmetric structure of the dominant chamber in SLV may affect the blood streamline in LV.

Limitations

Since the A wave fused into the E wave in many children in the study, we did not discuss these parameters in our article. Not only the impairment of cardiac function but also the preload, volume, and atrial and ventricular stiffness influence the results, but it is difficult to distinguish them completely. The shape of the ventricle and anatomic structures such as valve and papillary muscle may affect the turning of streamlines and the formation of the vortices, while in our study, valves and papillary muscles were smoothed out to optimize CFD modeling. Our sample size of this study was relatively small. Furthermore, more patients and long-term follow-up are needed for further study.

Conclusion

Both SLV and TA have impaired systolic and diastolic function. Patients with SLV have poorer cardiac function than those with TA due to less compensation and more disordered streamline. Our study demonstrates that twist is a good indicator for measuring ventricular performance, which may predate more noticeable echocardiographic signs of deterioration.

Data availability statement

The raw data supporting the conclusions of this article will be made available by the authors, without undue reservation.

Ethics statement

The studies involving human participants were reviewed and approved by regional research ethics committee (REC) of Shanghai Children's Medical Center Affiliated to Shanghai Jiao Tong University School of Medicine. Written informed consent to participate in this study was provided by the participants' legal guardian/next of kin.

References

- Warnes CA, Williams RG, Bashore TM, Child JS, Connolly HM, Dearani JA, et al. ACC/AHA 2008 guidelines for the management of adults with congenital heart disease: a report of the American College of Cardiology/American Heart Association Task Force on practice guidelines (writing committee to develop guidelines on the management of adults with congenital heart disease). Developed in collaboration with the American Society of Echocardiography, Heart Rhythm Society, International Society for Adult Congenital Heart Disease, Society for Cardiovascular Angiography and Interventions, and Society of Thoracic Surgeons. *J Am Coll Cardiol.* (2008) 52:e143–263. doi: 10.1016/j.jacc.2008.10.001
- Cheung YF, Penny DJ, Redington AN. Serial assessment of left ventricular diastolic function after Fontan procedure. *Heart.* (2000) 83:420–4. doi: 10.1136/heart.83.4.420
- Alsoufi B, Gillespie S, Kim D, Shashidharan S, Kanter K, Maher K, et al. The impact of dominant ventricle morphology on palliation outcomes of single ventricle anomalies. *Ann Thorac Surg.* (2016) 102:593–601. doi: 10.1016/j.athoracsur.2016.04.054
- Vitanova K, Shiraishi S, Mayr B, Beran E, Cleuziou J, Strbad M, et al. Impact of characteristics at stage-2-palliation on outcome following Fontan completion. *Pediatr Cardiol.* (2019) 40:1476–87. doi: 10.1007/s00246-019-02172-6
- Tweddell JS, Nersesian M, Mussatto KA, Nugent M, Simpson P, Mitchell ME, et al. Fontan palliation in the modern era: factors impacting mortality and morbidity. *Ann Thorac Surg.* (2009) 88:1291–9. doi: 10.1016/j.athoracsur.2009.05.076
- Kamata M, Stiver C, Naguib A, Tumin D, Tobias JD. A retrospective analysis of the influence of ventricular morphology on the perioperative outcomes after Fontan surgery. *J Cardiothorac Vasc Anesth.* (2017) 31:128–33. doi: 10.1053/j.jvca.2016.07.024
- Baltabaeva A, Marciniak M, Bijmens B, Moggridge J, He FJ, Antonios TF, et al. Regional left ventricular deformation and geometry analysis provides insights in myocardial remodelling in mild to moderate hypertension. *Eur J Echocardiogr.* (2008) 9:501–8. doi: 10.1016/j.euje.2007.08.004
- Rösner A, Khalapyan T, Dalen H, McElhinney DB, Friedberg MK, Lui GK. Classic-pattern dyssynchrony in adolescents and adults with a Fontan circulation. *J Am Soc Echocardiogr.* (2018) 31:211–9. doi: 10.1016/j.echo.2017.10.018
- Dorobantu DM, Wadey CA, Amir NH, Stuart AG, Williams CA, Pieleas GE. The role of speckle tracking echocardiography in the evaluation of common inherited cardiomyopathies in children and adolescents: a systematic review. *Diagnostics.* (2021) 11:635. doi: 10.3390/diagnostics11040635

Author contributions

L-JC and L-PW: data acquisition, analysis and interpretation of data, and writing original draft. L-SZ: data analysis of 3DSTE, Z-FZ: data analysis of 2D echocardiography. J-LL: data analysis of CFD. W-JH and S-WZ: data acquisition. S-FB: methodology. JY and Y-QZ: conception and design of the study, writing, review, and editing. All authors contributed to the article and approved the submitted version.

Funding

We express our great gratitude for the support from the National Natural Science Foundation of China (No. 82001835, 81970439), the Biomedical and Engineering (Science) Interdisciplinary Study Fund of Shanghai Jiao Tong University (No. G2019QNB03), SJTU Trans-med Awards Research (No. 20220101), and the Innovative Research Team of High-Level Local Universities in Shanghai.

Conflict of interest

The authors declare that the research was conducted in the absence of any commercial or financial relationships that could be construed as a potential conflict of interest.

Publisher's note

All claims expressed in this article are solely those of the authors and do not necessarily represent those of their affiliated organizations, or those of the publisher, the editors and the reviewers. Any product that may be evaluated in this article, or claim that may be made by its manufacturer, is not guaranteed or endorsed by the publisher.

10. Zhong SW, Zhang YQ, Chen LJ, Wang SS, Li WH. Evaluation of left ventricular volumes and function by real time three-dimensional echocardiography in children with functional single left ventricle: a comparison between QLAB and TomTec. *Echocardiography*. (2015) 32:1554–63. doi: 10.1111/echo.12990
11. Zhong SW, Zhang YQ, Chen LJ, Wang SS, Li WH, Sun YJ. Ventricular twisting and dyssynchrony in children with single left ventricle using three-dimensional speckle tracking imaging after the Fontan operation. *Echocardiography*. (2016) 33:606–17. doi: 10.1111/echo.13103
12. Chen LJ, Tong ZR, Wang Q, Zhang YQ, Liu JL. Feasibility of computational fluid dynamics for evaluating the intraventricular hemodynamics in single right ventricle based on echocardiographic images. *Biomed Res Int*. (2018) 2018:1042038. doi: 10.1155/2018/1042038
13. Karabulut A, Doğan A, Tuzcu AK. Myocardial performance index for patients with overt and subclinical hypothyroidism. *Med Sci Monit*. (2017) 23:2519–26. doi: 10.12659/msm.905190
14. Yang HS. Three-dimensional echocardiography in adult congenital heart disease. *Korean J Intern Med*. (2017) 32:577–88. doi: 10.3904/kjim.2016.251
15. Eskofier J, Wefstaedt P, Beyerbach M, Nolte I, Hungerbühler SO. Quantification of left ventricular volumes and function in anesthetized beagles using real-time three-dimensional echocardiography: 4D-TomTec™ analysis versus 4D-AutLVQ™ analysis in comparison with cardiac magnetic resonance imaging. *BMC Vet Res*. (2015) 11:260. doi: 10.1186/s12917-015-0568-5
16. Shrout PE, Fleiss JL. Intraclass correlations: uses in assessing rater reliability. *Psychol Bull*. (1979) 86:420–8. doi: 10.1037//0033-2909.86.2.420
17. Mohammed A, Mertens L, Friedberg MK. Relations between systolic and diastolic function in children with dilated and hypertrophic cardiomyopathy as assessed by tissue Doppler imaging. *J Am Soc Echocardiogr*. (2009) 22:145–51. doi: 10.1016/j.echo.2008.11.010
18. Hershenson JA, Zaidi AN, Texter KM, Moiduddin N, Stefaniak CA, Hayes J, et al. Differences in tissue Doppler imaging between single ventricles after the Fontan operation and normal controls. *Am J Cardiol*. (2010) 106:99–103. doi: 10.1016/j.amjcard.2010.02.020
19. Ezon DS, Maskatia SA, Sexson-Tejtel K, Dreyer WJ, Jewea A, Denfield SW. Tissue Doppler imaging measures correlate poorly with left ventricular filling pressures in pediatric cardiomyopathy. *Congenit Heart Dis*. (2015) 10:E203–9. doi: 10.1111/chd.12267
20. Dragulescu A, Mertens L, Friedberg MK. Interpretation of left ventricular diastolic dysfunction in children with cardiomyopathy by echocardiography: problems and limitations. *Circ Cardiovasc Imaging*. (2013) 6:254–61. doi: 10.1161/circimaging.112.000175
21. Appleton CP, Firstenberg MS, Garcia MJ, Thomas JD. The echo-Doppler evaluation of left ventricular diastolic function. A current perspective. *Cardiol Clin*. (2000) 18:513–46, ix. doi: 10.1016/s0733-8651(05)70159-4
22. Rios R, Ginde S, Saudek D, Looma RS, Stelter J, Frommelt P. Quantitative echocardiographic measures in the assessment of single ventricle function post-Fontan: incorporation into routine clinical practice. *Echocardiography*. (2017) 34:108–15. doi: 10.1111/echo.13408
23. Campbell MJ, Quartermain MD, Cohen MS, Faerber J, Okunowo O, Wang Y, et al. Longitudinal changes in echocardiographic measures of ventricular function after Fontan operation. *Echocardiography*. (2020) 37:1443–8. doi: 10.1111/echo.14826
24. La Corte MA, Dick M, Scheer G, La Farge CG, Fyler DC. Left ventricular function in tricuspid atresia. Angiographic analysis in 28 patients. *Circulation*. (1975) 52:996–1000. doi: 10.1161/01.cir.52.6.996
25. Ruzicka M, Keeley FW, Leenen FH. The renin-angiotensin system and volume overload-induced changes in cardiac collagen and elastin. *Circulation*. (1994) 90:1989–96. doi: 10.1161/01.cir.90.4.1989
26. Konstam MA, Kramer DG, Patel AR, Maron MS, Udelson JE. Left ventricular remodeling in heart failure: current concepts in clinical significance and assessment. *JACC Cardiovasc Imaging*. (2011) 4:98–108. doi: 10.1016/j.jcmg.2010.10.008
27. Moiduddin N, Texter KM, Zaidi AN, Hershenson JA, Stefaniak C, Hayes J, et al. Two-dimensional speckle strain and dyssynchrony in single left ventricles vs. normal left ventricles. *Congenit Heart Dis*. (2010) 5:579–86. doi: 10.1111/j.1747-0803.2010.00460.x
28. Schmid P, Jaermann T, Boesiger P, Niederer PF, Lunkenheimer PP, Cryer CW, et al. Ventricular myocardial architecture as visualised in postmortem swine hearts using magnetic resonance diffusion tensor imaging. *Eur J Cardiothorac Surg*. (2005) 27:468–72. doi: 10.1016/j.ejcts.2004.11.036
29. Sanchez-Quintana D, Climent V, Ho SY, Anderson RH. Myoarchitecture and connective tissue in hearts with tricuspid atresia. *Heart*. (1999) 81:182–91. doi: 10.1136/hrt.81.2.182
30. Lunze FI, Lunze K, McElhinney DB, Colan SD, Gauvreau K, Lange PE, et al. Heterogeneity of regional function and relation to ventricular morphology in patients with Fontan circulation. *Am J Cardiol*. (2013) 112:1207–13. doi: 10.1016/j.amjcard.2013.06.016
31. Weidemann F, Herrmann S, Störk S, Niemann M, Frantz S, Lange V, et al. Impact of myocardial fibrosis in patients with symptomatic severe aortic stenosis. *Circulation*. (2009) 120:577–84. doi: 10.1161/circulationaha.108.847772
32. Weidemann F, Niemann M, Herrmann S, Kung M, Störk S, Waller C, et al. A new echocardiographic approach for the detection of non-ischaemic fibrosis in hypertrophic myocardium. *Eur Heart J*. (2007) 28:3020–6. doi: 10.1093/eurheartj/ehm454
33. Rathod RH, Prakash A, Powell AJ, Geva T. Myocardial fibrosis identified by cardiac magnetic resonance late gadolinium enhancement is associated with adverse ventricular mechanics and ventricular tachycardia late after Fontan operation. *J Am Coll Cardiol*. (2010) 55:1721–8. doi: 10.1016/j.jacc.2009.12.036
34. Phan TT, Shivu GN, Abozguia K, Sanderson JE, Frenneaux M. The pathophysiology of heart failure with preserved ejection fraction: from molecular mechanisms to exercise haemodynamics. *Int J Cardiol*. (2012) 158:337–43. doi: 10.1016/j.ijcard.2011.06.113
35. Bing R, Dweck MR. Myocardial fibrosis: why image, how to image and clinical implications. *Heart*. (2019) 105:1832–40. doi: 10.1136/heartjnl-2019-315560
36. Ho SY, Jackson M, Kilpatrick L, Smith A, Gerlis LM. Fibrous matrix of ventricular myocardium in tricuspid atresia compared with normal heart. A quantitative analysis. *Circulation*. (1996) 94:1642–6. doi: 10.1161/01.cir.94.7.1642
37. Ho PK, Lai CT, Wong SJ, Cheung YF. Three-dimensional mechanical dyssynchrony and myocardial deformation of the left ventricle in patients with tricuspid atresia after fontan procedure. *J Am Soc Echocardiogr*. (2012) 25:393–400. doi: 10.1016/j.echo.2012.01.003
38. Badano LP, Muraru D. Twist mechanics of the left ventricle. *Circ Cardiovasc Imaging*. (2019) 12:e009085. doi: 10.1161/circimaging.119.009085
39. Thomas JD, Weyman AE. Echocardiographic Doppler evaluation of left ventricular diastolic function. Physics and physiology. *Circulation*. (1991) 84:977–90. doi: 10.1161/01.cir.84.3.977
40. Khoo NS, Smallhorn JF, Kaneko S, Kutty S, Altamirano L, Tham EB. The assessment of atrial function in single ventricle hearts from birth to Fontan: a speckle-tracking study by using strain and strain rate. *J Am Soc Echocardiogr*. (2013) 26:756–64. doi: 10.1016/j.echo.2013.04.005
41. Brooks PA, Khoo NS, Hornberger LK. Systolic and diastolic function of the fetal single left ventricle. *J Am Soc Echocardiogr*. (2014) 27:972–7. doi: 10.1016/j.echo.2014.06.012
42. Mor-Avi V, Jenkins C, Kühl HP, Nesser HJ, Marwick T, Franke A, et al. Real-time 3-dimensional echocardiographic quantification of left ventricular volumes: multicenter study for validation with magnetic resonance imaging and investigation of sources of error. *JACC Cardiovasc Imaging*. (2008) 1:413–23. doi: 10.1016/j.jcmg.2008.02.009
43. Binotto MA, Higuchi Mde L, Aiello VD. Left ventricular remodeling in hearts with tricuspid atresia: morphologic observations and possible basis for ventricular dysfunction after surgery. *J Thorac Cardiovasc Surg*. (2003) 126:1026–32. doi: 10.1016/s0022-5223(03)00696-2
44. Lopez C, Mertens L, Dragulescu A, Landeck B, Younoszai A, Friedberg MK, et al. Strain and rotational mechanics in children with single left ventricles after fontan. *J Am Soc Echocardiogr*. (2018) 31:1297–306. doi: 10.1016/j.echo.2018.09.004
45. D'Alto M, Scognamiglio G, Dimopoulos K, Bossone E, Vizza D, Romeo E, et al. Right heart and pulmonary vessels structure and function. *Echocardiography*. (2015) 32(Suppl 1):S3–10. doi: 10.1111/echo.12227
46. Pedrizzetti G, Domenichini F. Nature optimizes the swirling flow in the human left ventricle. *Phys Rev Lett*. (2005) 95:108101. doi: 10.1103/PhysRevLett.95.108101